JAK-STAT pathway activation compromises nephrocyte function in a *Drosophila* high-fat diet model of chronic kidney disease

Yunpo Zhao[1,2], Jianli Duan[1,2], Joyce van de Leemput[1,2], and Zhe Han[1,2,*]

1. Center for Precision Disease Modeling, Department of Medicine, University of Maryland School of Medicine, Baltimore, MD 21201, USA
2. Division of Endocrinology, Diabetes and Nutrition, Department of Medicine, University of Maryland School of Medicine, Baltimore, MD 21201, USA

* Corresponding author: Dr. Zhe Han, Center for Precision Disease Modeling, Department of Medicine, University of Maryland School of Medicine, 670 West Baltimore Street, Baltimore, MD 21201, USA; email: zhan@som.umaryland.edu

Running title: JAK-STAT in high-fat diet dysfunctional nephrocytes

HIGHLIGHTS

- High-fat diet (HFD) disrupt nephrocyte slit diaphragm structure and filtration
- HFD releases fat body adipokine, Upd2, which activates JAK-STAT in nephrocytes
- Genetic/pharmacological inhibition of JAK-STAT reverses HFD nephrocyte dysfunction
- JAK-STAT signaling mediates adipose-nephrocyte axis in HFD-associated nephropathy

IMPACT STATEMENT

Using a *Drosophila* model for chronic kidney disease, Zhao et al. show that a high-fat diet induces excretion of a leptin-like JAK-STAT ligand from the fat body. Thus, driving the adipose-nephrocyte (podocyte equivalent) axis through activated JAK-STAT signaling. These findings link obesity to kidney disease, implicating new avenues for therapeutics.

ABSTRACT

Chronic kidney disease is a major healthy issue and is gaining prevalence. Using a *Drosophila* model for chronic kidney disease we show that a high-fat diet (HFD) disrupts the slit diaphragm filtration structure in nephrocytes, the fly functional equivalent of mammalian podocytes. The structural disruption resulted in reduced filtration function in the affected nephrocytes. We demonstrate that a HFD activates the JAK-STAT pathway in nephrocytes, which has previously been linked to diabetic kidney disease. JAK-STAT activation was initiated by increased expression and release of the adipokine, Upd2, from the fat body. This leptin-like hormone is a known ligand of JAK-STAT. Both genetic and pharmacological inhibition of JAK-STAT restored nephrocyte HFD-associated dysfunction. Altogether, our study reveals the importance of the JAK-STAT signaling pathway in the adipose tissue−nephrocyte axis and its contribution to HFD-associated nephropathy. These findings open new avenues for intervention in treating diabetic nephropathy and chronic kidney disease.

INTRODUCTION

Chronic kidney disease is a prevalent health issue, with an estimated ~12% of people affected worldwide, many of whom are unaware of their condition (Coresh, 2017; US Department of Health and Human Services, Centers for Disease Control and Prevention (Atlanta, GA), 2023). The gradual loss of kidney function results in excess fluid and buildup of metabolic waste compounds. Clinical symptoms include atherosclerosis, chronic inflammation, malnutrition, and insulin resistance among other metabolic imbalances (Serrano et al., 2023). Altogether these lead to increased morbidity and mortality associated with chronic kidney failure (GBD Chronic Kidney Disease Collaboration, 2020). Diabetes, high blood pressure, ageing, obesity, and increased BMI are major risk factors for glomerulopathy and chronic kidney disease (Alizadeh et al., 2019; Berthoux et al., 2013; Bonnet et al., 2001; Coresh, 2017; Hsu et al., 2006; Moorhead et al., 1982; Tsuboi et al., 2013). Notably, patients with primary kidney disease that are also obese have worsened outcomes (Berthoux et al., 2013) and following kidney transplantation patients with increased BMI are at greater risk of adverse outcomes (Curran et al., 2014). with risk increasing risk as BMI increases (Hsu et al., 2006). The link between dietary fat intake and kidney disease has raised interest into the adipose-renal axis; that is how do bodily fat deposits affect kidney function?

Podocytes from patients with chronic kidney disease contain lipid droplets that store excess fat (Herman-Edelstein et al., 2014; Kimmelstiel and Wilson, 1936), these cause lipotoxicity by disrupting the mitochondria, as well as endocytosis (Lubojemska et al., 2021), a process crucial to the kidney filtration structure (Wang et al., 2021). Studies in rats and mice on a HFD have repeatedly shown that the animals suffer from obesity, diabetes (altered insulin homeostasis), and kidney injury marked by functional (albuminuria; blood accumulation of BUN and creatinine; increased urinary biomarkers of kidney damage) and structural (glomerulopathy with glomerular hypertrophy and focal segmental glomerulosclerosis; fibrosis) deficiencies (Altunkaynak et al., 2008; Ha et al., 2022; Jiang et al., 2005; Kuwahara et al., 2016; Lu et al., 2003; Rangel Silvares et al., 2019; Ruggiero et al., 2011; Sánchez-Navarro et al., 2021; Sun et al., 2020; Szeto et al., 2016; van der Heijden et al., 2015). Like in patients with chronic kidney disease, lipid droplets have been observed in the kidneys of HFD rats and mice (Deji et al., 2009; Jiang et al., 2005; Sun et al., 2020; van der Heijden et al., 2015) and have been associated with dysfunctional cellular systems including oxidative stress, renal inflammation, ER-stress, disruption of mitochondrial dynamics, and impaired autophagy-lysosomal pathway in the cells of the kidneys (Cai et al., 2024; Ha et al., 2022; Kuwahara et al., 2016; C. Li et al., 2016; Lu et al., 2003; Rangel Silvares et al., 2019; Ruggiero et al., 2011; Sánchez-Navarro et al., 2021; Sun et al., 2020; Szeto et al., 2016; van der Heijden et al.,

111 2015). Altogether, these indicate the involvement of both local and systemic changes (Deji et
112 al., 2009). However, our understanding of the pathways that govern the pathogenic effect of
113 superfluous fat intake on kidney function, as well as how to leverage this knowledge to develop
114 effective therapeutics, remains incomplete.
115
116 Recently, an HFD model in *Drosophila* showed lipotoxicity, i.e. lipid droplet accumulation, in
117 the fly nephrocytes (Lubojemska et al., 2021). Nephrocytes share many characteristics with
118 human podocytes, including genetics, molecular pathways, and function (Weavers et al.,
119 2009; Zhang et al., 2013b, 2013a). Both cell types contain highly specialized filtration
120 structures know as slit diaphragms that act in concert with the basement membrane; the fly
121 lacuna channel is similar to the urinary space in the mammalian Bowman's capsule; and, many
122 key proteins for podocyte function are likewise essential for nephrocyte function (van de
123 Leemput et al., 2022; Wang et al., 2021; Weavers et al., 2009; Zhuang et al., 2009). Indeed,
124 fly in vivo nephrocyte models have been successfully used to study a variety of human kidney
125 diseases, including forms of monogenic nephrotic syndrome and steroid-resistant nephrotic
126 syndrome (SRNS) (Ashraf et al., 2013; Bierzynska et al., 2022; Fu et al., 2017; Gee et al.,
127 2015, 2013; Gonçalves et al., 2018; Hermle et al., 2018, 2017; Milosavljevic et al., 2022;
128 Odenthal et al., 2023; Paul et al., 2023; Zhao et al., 2019; Zhu et al., 2017). The recent study
129 using the HFD Drosophila model recapitulated the ectopic lipid droplets and cellular
130 dysfunction observed in chronic kidney disease and found that the adipose-derived triglyceride
131 lipase protects nephrocyte endocytosis under HFD conditions (Lubojemska et al., 2021). Here,
132 we used an HFD *Drosophila melanogaster* model of chronic kidney disease to investigate the
133 role and factors of the adipose-renal axis in chronic kidney disease and identified Upd-
134 activated JAK-STAT signaling as a key component.
135
136
137 **RESULTS**
138
139 **High-fat diet (HFD) compromises nephrocyte function**
140 To investigate the effect of superfluous fat consumption on nephrocyte function, newly eclosed
141 flies were fed a normal fat diet (NFD) or a high-fat diet (HFD) for seven days. Then, the flies
142 were subjected to fluorescent dye uptake assays to determine nephrocyte function. Compared
143 to the NFD fed flies, the HFD fed flies showed reduced FITC conjugated albumin (FITC-
144 albumin, 66 kD) fluorescence (Figure 1A and B). Likewise, HFD feeding significantly reduced
145 10 kD dextran uptake by the nephrocytes (Figure 1C and D). Thus, confirming the HFD model
146 in *Drosophila* for studying kidney disease (Lubojemska et al., 2021) and demonstrating that in
147 our hands the consumption of superfluous fat caused nephrocyte uptake dysfunction.

148

149 **HFD alters nephrocyte morphology**

150 The slit diaphragm (SD) is the fundamental filtration structure of nephrocytes. Thus, given the
151 HFD-induced dysfunctional uptake, we next tested whether the SD is affected by HFD.
152 Therefore we looked at the distribution of polychaetoid (Pyd), the fly homolog of human tight
153 junction protein 1 (TJP1, alias ZO-1) and a key component of the SD filtration unit (van de
154 Leemput et al., 2022). Immunostaining with anti-Pyd antibody showed predominant
155 membrane localization of Pyd in nephrocytes from NFD fed flies. At the cortical surface of NFD
156 nephrocytes, Pyd showed the fingerprint-like pattern characteristic of the SD (Figure 2A).
157 However, in the HFD fed flies, the SD fingerprint-like pattern appeared irregular and Pyd
158 showed an uneven distribution with spots of increased signal intensity (Figure 2A). These
159 might correlate to the trails of Pyd seemingly hanging from the cortical surface inside the HFD
160 nephrocytes, along with cytosolic accumulation of Pyd protein (Figure 2A and B). These
161 findings show that a HFD leads to structural disruption of the SD filtration unit in nephrocytes,
162 that likely accounts for the nephrocyte functional deficit observed earlier.

163

164 To study the nephrocyte SD and cytoplasmic regions in more detail, we performed
165 transmission electron microscopy (TEM). The nephrocytes of NFD fed flies showed regularly
166 arranged lacuna channels along the cortical surface (Figure 2C). The distance between the
167 lacuna channels was significantly increased in nephrocytes from HFD fed flies (Figure 2C and
168 D). Nephrocytes from both NFD and HFD fed flies showed big subcellular vacuoles (Figure
169 2E). However, the vacuoles in NFD nephrocytes frequently contained electron dense
170 structures, whereas most vacuoles in HFD nephrocytes were clear (Figure 2E and F).
171 Altogether, these findings demonstrate that a HFD causes significant changes to the
172 nephrocyte and its SD, both at the cortical and subcortical levels.

173

174 **HFD potentiates the JAK-STAT pathway in nephrocytes**

175 Activity of the Janus kinase/signal transducer and activator of transcription (JAK-STAT)
176 pathway has been linked to diabetic kidney disease (Berthier et al., 2009), likewise it is
177 activated systemically in *Drosophila* in response to a chronic lipid-rich diet (Woodcock et al.,
178 2015). Key components of the JAK-STAT pathway are conserved in fly, including *Signal-*
179 *transducer and activator of transcription protein at 92E* (*Stat92E*), *hopscotch* (*hop*), *domeless*
180 (*dome*), and *Suppressor of cytokine signaling at 36E* (*Socs36E*) (Figure 3A and B). Therefore,
181 we tested whether the JAK-STAT pathway was activated in the nephrocytes of HFD-fed flies.
182 We used a fluorescent reporter *10xStat92E*-GFP of JAK-STAT pathway activity (Ekas et al.,
183 2006). Low levels of *Stat92E*-GFP fluorescence were detected in the nephrocytes of flies on
184 a regular diet (NFD). However, in nephrocytes from HFD-fed flies, the fluorescence was

185 significantly increased (Figure 3C and D). These findings indicate that the consumption of
186 superfluous fat indeed activates the JAK-STAT pathway in nephrocytes.
187
188 **Activation of the Janus kinase, Hop, reduces nephrocyte function**
189 Since JAK-STAT signaling has been shown to play an important role during development
190 (Brown et al., 2001; Liu et al., 2009), we wanted to isolate its requirement for mature
191 nephrocyte filtration function. To do this we used a dominant gain-of-function allele of *hop*
192 (*Tumorous-lethal*, *hop.Tum*); a single amino acid change (Gly341Glu) whose expression leads
193 to JAK-STAT pathway activation (Harrison et al., 1995). We expressed *UAS-hop.Tum*
194 specifically in mature nephrocytes using a temperature sensitive *Dot*-Gal4 driver (*Dot*-Gal4*;*
195 *tub*-Gal80ts, referred to as *Dot*-Gal4ts), known as the TARGET system (McGuire et al., 2004),
196 to turn on expression in adult flies specifically as they are switched to a different environmental
197 temperature (Figure 4A). Overexpression of *hop.Tum* significantly reduced nephrocyte
198 absorption ability in the adults, as shown with reduced FITC-albumin and 10 kD dextran in
199 *Dot*-Gal4ts>UAS-*hop.Tum* nephrocytes compared with control nephrocytes (Figure 4B-E).
200
201 To validate these results and remove between-fly variability, both biological and technical, we
202 also tested the effect of JAK-STAT pathway activation in tissue mosaic clones using Flp-out
203 (Duan et al., 2020) (Figure 4F). For this technique first instar larvae are exposed to heat shock
204 to activate the Hsp70P transcription factor, which induces *Flippase* (*Flp*). Flp activity in turn,
205 removes the stop-cassette thereby freeing *Gal4*. Gal4 drives the expression of UAS-GFP and
206 UAS-*hop.tum* within the same cell. Thus, Gal4 and therefore *hop.Tum* is only expressed in
207 GFP-labelled nephrocyte clones; whereas, GFP-negative nephrocytes are indicative of no
208 Gal4 being expressed and serve as internal control cells (Figure 4F). In line with the TARGET
209 assays, UAS-*hop.Tum* overexpression significantly reduced nephrocyte absorption ability in
210 adult flies (Figure 4G and H). These data support a role for JAK-STAT pathway in nephrocyte
211 function.
212
213 **Depletion of Socs36E, a negative regulator of JAK-STAT, or increased adipokine Upd2,**
214 **a JAK-STAT ligand, result in decreased nephrocyte function**
215 Next, we looked at additional JAK-STAT pathway components in the context of nephrocyte
216 function. Suppressor of cytokine signaling at 36E (Socs36E) is transcriptionally regulated by
217 Signal-transducer and activator of transcription 92E (Stat92E) and functions as a negative
218 regulator of JAK-STAT signaling (Callus and Mathey-Prevot, 2002; Karsten et al., 2002)
219 (Figure 3B) and it is expressed in the nephrocytes (Figure 3A). Silencing *Socs36E* specifically
220 in nephrocytes (*Dot*-Gal4>*Socs36E*-RNAi) significantly reduced nephrocyte uptake function

221 as evident in significantly decreased FITC-albumin (Figure 5A and B) and 10 kD dextran
222 (Figure 5C and D) fluorescence compared to the control nephrocytes.
223
224 In *Drosophila*, the JAK-STAT pathway ligand unpaired (Upd) family is encoded by *upd1*, *upd2*,
225 and *upd3*. These ligands bind to Domeless (Dome), a single-transmembrane receptor, to
226 activate JAK-STAT signaling (Figure 3B). Of these, Upd2 is functionally equivalent to human
227 Leptin and is highly expressed in the fat body, the fly's functional equivalent of vertebrate
228 adipose tissue (Hombria et al., 2005; Rajan et al., 2017; Rajan and Perrimon, 2012). In
229 *Drosophila*, HFD has been shown to upregulate Upd2 expression and secretion (Rajan et al.,
230 2017; Rajan and Perrimon, 2012). In our model, over-expression of Upd2, specifically in the
231 fat body (*ppl*-Gal4 driver; *ppl*-Gal4>*upd2*-GFP), significantly reduced 10 kD dextran uptake in
232 the nephrocytes compared to the control (*ppl*-Gal4/+) (Figure 5E and F), indicating reduced
233 nephrocyte function. Note, since our *upd2* over-expression line contains *upd2*-GFP, we could
234 not use the FITC-albumin uptake assay, as both signals occupy the same imaging channel.
235
236 Like the Janus kinase Hop, the negative regulator Socs36E and the ligand adipokine Upd2
237 are additional JAK-STAT pathway components that are required for nephrocyte function.
238
239 **HFD-induced nephrocyte functional defects are mitigated by Stat92E-mediated**
240 **inhibition of JAK-STAT**
241 To determine that JAK-STAT forms a direct link between HFD and nephrocyte dysfunction,
242 we knocked down *Stat92E* (*Stat92E*-IR (Recasens-Alvarez et al., 2017)) in the nephrocytes
243 to disrupt the JAK-STAT signaling pathway (Figure 3B). Deficiency for Stat92E did not affect
244 the uptake function (FITC-albumin or 10 kD dextran) of adult nephrocytes in flies fed a NFD
245 (Figure 6A-D). However, under HFD conditions, in which nephrocytes from control flies
246 showed significantly reduced uptake, *Stat92D* deficient nephrocytes showed FITC-albumin
247 and 10 kD dextran fluorescence restored to NFD levels (Figure 6A-D). These findings
248 demonstrate that Stat92E, and by extension the JAK-STAT pathway, is required for the
249 nephrocyte dysfunction induced by HFD.
250
251 **HFD-induced nephrocyte functional defects can be attenuated by methotrexate**
252 **treatment**
253 Methotrexate suppresses STAT activation; it inhibits the phosphorylation of JAK which is
254 necessary for JAK-STAT pathway activation, and was shown to do so without affecting other
255 phosphorylation-dependent pathways (Thomas et al., 2015). In our model system,
256 methotrexate treatment (10 μM; 60 min) reduced levels of Stat92E (10xStat92E-GFP) in the
257 nephrocytes (Supplementary figure S1). Stat92E is a key component of the pathway, its

reduction is indicative of decreased JAK-STAT signaling. Next, we treated flies on NFD or HFD with 10 μM methotrexate (60 min incubation; ex vivo) to study the effect of pharmacological JAK-STAT inhibition on nephrocyte function. In nephrocytes from control flies on a regular diet (NFD), the methotrexate treatment had no effect on uptake of FITC-albumin or 10 kD dextran (Figure 7A-D). However, in flies on a HFD, treatment with methotrexate led to significantly increased nephrocyte FITC-albumin and 10 kD dextran uptake, restoring levels to those observed in control fly NFD nephrocytes (Figure 7A-D). Thus, like the genetic intervention (*Stat92E* inhibition; Figure 6), pharmacological intervention with the JAK-STAT inhibitor methotrexate restored nephrocyte function caused by HFD. These findings support the notion that HFD-induced nephrocyte dysfunction is mediated by the JAK-STAT signaling pathway.

Keywords

JAK-STAT; Upd2; Leptin; high-fat diet; nephropathy; chronic kidney disease; *Drosophila*

DISCUSSION

A recent publication showed that flies fed a HFD can recapitulate key features of chronic kidney disease, including lipid droplet formation, altered mitochondria dynamics, and endocytosis defects observed as reduced uptake of dextran and albumin (Lubojemska et al., 2021). This previous study found that excess fatty acids, a sign of lipotoxicity, due to a HFD are released from adipose tissue into circulation, then filtered out by the nephrocytes by receptor-mediated endocytosis, at which point the fatty acids accumulate in the lipid droplets (Lubojemska et al., 2021); like those observed in the podocytes of patients with chronic kidney disease (Herman-Edelstein et al., 2014; Kimmelstiel and Wilson, 1936). Notably, lipid droplet lipolysis could counteract the HFD-induced disrupted endocytosis in the nephrocytes via the mitochondria (Lubojemska et al., 2021). This demonstrated one mechanism by which excess lipid droplets, due to HFD, can disrupt nephrocyte kidney function. Here, we likewise used a HFD *Drosophila* model to study chronic kidney disease and revealed another mechanism by which HFD affects both nephrocyte uptake function and morphology of its filtration structure, the slit diaphragm. HFD upregulates the expression of the adipokine Upd2, the functional homolog to human Leptin, which activates the JAK-STAT pathway (Rajan and Perrimon, 2012). Our data show this also holds true in the nephrocytes, and as such compromises nephrocyte function (Figure 7E). These findings support obesity as a causal factor in chronic kidney disease.

295 Of note, in early stage diabetic kidney disease, JAK-STAT pathway genes are upregulated in
296 patient podocytes (Berthier et al., 2009). In a rat diabetic model, treatment with a JAK-STAT
297 inhibitor (AG-490) reduced proteinuria (Banes et al., 2004); and, overexpression of JAK2 in
298 diabetic mouse podocytes elevated JAK-STAT pathway activity and exacerbated diabetic
299 kidney disease (Zhang et al., 2017). These findings, like ours that showed effective treatment
300 of HFD nephropathy using the JAK-STAT inhibitor (methotrexate), support the involvement of
301 the JAK-STAT pathway in HFD-related chronic kidney disease. They also demonstrate that
302 this pathological effect is conserved from flies to mammals. In fact, a phase 2 clinical trial
303 demonstrated that the small molecule baricitinib, a selective JAK1 and JAK2 inhibitor,
304 effectively lowered albuminuria in patients with type 2 diabetes and diabetic kidney disease
305 (Tuttle et al., 2018). Altogether these studies support JAK-STAT inhibition as a therapeutic
306 intervention for nephropathy associated with superfluous fat intake (Brosius et al., 2016). The
307 conserved disease mechanism makes the HFD fly model a valuable platform to screen JAK-
308 STAT inhibitors for their efficacy to treat chronic kidney disease. The fly findings showed a
309 direct JAK-STAT link at the adipose tissue−nephrocyte axis leads to nephrocyte dysfunction;
310 via HFD upregulated expression of the adipokine Upd2, which activates the JAK-STAT
311 pathway (Rajan and Perrimon, 2012) (Figure 7E). In support, like in our fly model, increased
312 leptin has been observed in obese patients (Considine et al., 1996) and in patients with chronic
313 renal failure (Heimbürger et al., 1997).
314
315 Finally, while growing evidence demonstrates that a pharmacological block of the JAK-STAT
316 pathway could effectively treat nephropathy, for decades, the first-line treatment for obesity-
317 related glomerulopathy has been RAS inhibitors (Jiang et al., 2023). Their beneficial effects
318 stemming from lowering blood pressure and by lowering the estimated glomerular filtration
319 rate (eGFR) (Banerjee et al., 2022; Yamout et al., 2014). One such inhibitor, telmisartan,
320 targets RAS by blocking the angiotensin (Ang) II receptor and was shown effective in treating
321 nephropathy in a rat model of metabolic syndrome (HFD-fed rats) (H. Li et al., 2016). Notably,
322 telmisartan treatment decreased leptin release from adipose tissue, thereby supporting our
323 model and implicating a hitherto unknown mechanism contributes to leptin-associated
324 nephropathy in metabolic syndrome. In addition, our findings could have implications for lupus
325 nephritis, an inflammatory kidney disease associated with the autoimmune disease systemic
326 lupus erythematosus. Patients with this complication show activated JAK-STAT and elevated
327 leptin, regulated by Sterol regulatory element bending transcription factor 1 (SREBF1) which
328 is involved in lipogenesis (Hao et al., 2013). Already, phase 2/3 clinical trials are underway to
329 study the efficacy of JAK inhibitors in treating lupus nephritis (Huo et al., 2023). Our data
330 indicate a possible second pathway could contribute, by direct leptin stimulation of JAK-STAT
331 caused by the dysregulated fat body, warranting further investigation.

332

333 Altogether, our study expands our understanding of chronic kidney disease associated with
334 superfluous fat intake and provides new avenues for therapeutic strategies.

335

336

337 **MATERIALS AND METHODS**

338

339 **Key resources table**

REAGENT or RESOURCE	SOURCE	IDENTIFIER
Antibodies		
Chicken anti-GFP	Abcam	Cat. ab13970; RRID:AB_300798
Mouse monoclonal anti-Pyd	Developmental Studies Hybridoma Bank (DSHB)	RRID:AB_2618043
Goat anti-mouse Alexa fluor 488	Invitrogen	Cat. A11029; RRID:AB_2534088
Goat anti-chicken Alexa fluor 488	Invitrogen	Cat. A11039; AB_2534096
Chemicals, Peptides, and Recombinant Proteins		
DAPI	Thermo Fisher Scientific	Cat. D1306
Methotrexate	Sigma-Aldrich	Cas. 06563
10 kD Texas Red-dextran	Thermo Fisher Scientific	Cas. D1828
FITC-albumin solution	Sigma	Cas. A9771
Experimental Models: Organisms/Strains		
Drosophila melanogaster: w^{1118}	Bloomington Drosophila Stock Center (BDSC)	RRID: BDSC_3605
Drosophila melanogaster: *Dot*-Gal4	BDSC	RRID: BDSC_67608
Drosophila melanogaster: *ppl*-Gal4	BDSC	RRID: BDSC_58768
Drosophila melanogaster: *tub*-Gal80ts	BDSC	RRID: BDSC_7017
Drosophila melanogaster: *10XStat92E*-GFP	BDSC	RRID: BDSC_26198
Drosophila melanogaster: *Socs36E*-IR	BDSC	RRID: BDSC_35036
Drosophila melanogaster: *Stat92E-IR*	Vienna *Drosophila* Resource Center (VDRC)	VDRC_106980
Drosophila melanogaster: UAS-*hop.Tum*	Harrison, et.al., 19955	N/A
Drosophila melanogaster: UAS-*upd2:GFP*	Hombria, et.al., 2005	N/A
Drosophila melanogaster: *hs-Flp*^{122}; UAS-*Flp*^{JD1}/CyO, *Act-GFP*^{JMR1}; *Act5C>CD2>Gal4*^{S}, UAS-*mCD8-GFP*^{LL6}/TM6b	Zhao, et.al., 2005	N/A
Software and Algorithms		
FIJI (ImageJ)	Schneider et al., 2012; https://imagej.net/Fiji/Downloads	Fiji-macOS
Adobe Illustrator	https://www.adobe.com/	Adobe Illustrator 2022

GraphPad Prism	https://www.graphpad.com/scientific-software/prism/	GraphPad Prism 9

340

341 ***Drosophila* husbandry**

342 Fly lines were reared on a normal fat diet (NFD; Nutri-Fly German formula; Genesee Scientific,
343 San Diego, CA) or a high-fat diet (HFD; NFD supplemented with 14% coconut oil), under
344 standard conditions (25°C, 60% humidity, 12h:12h dark:light cycle), unless otherwise stated.

345

346 *Drosophila* stocks w^{1118} (BDSC_3605), *Dot*-Gal4 (BDSC_67608), *ppl*-Gal4 (BDSC_58768),
347 *tub*-Gal80ts (BDSC_7017), *10XStat92E*-GFP (BDSC_26198), and UAS-*Socs36E*-RNAi
348 (BDSC_35036) were obtained from the Bloomington Drosophila Stock Center (BDSC). UAS-
349 *Stat92E*-RNAi (VDRC_106980) was obtained from the Vienna Drosophila Resource Center
350 (VDRC). UAS-*hop.Tum* was kindly provided by Prof. Norbert Perrimon (Harvard Medical
351 School, Boston, MA; Howard Hughes Medical Institute, Boston, MA). UAS-*upd2:GFP* has
352 been previously described (Hombria et al., 2005) and was kindly provided by Prof. Ylva
353 Engström (Stockholm University, Stockholm, Sweden). The Flp-out line *hs-Flp*^{122}; UAS-
354 *Flp*^{JD1}/CyO, *Act-GFP*^{JMR1}; *Act5C>CD2>Gal4*^{S}, UAS-*mCD8-GFP*^{LL6}/TM6b was generated
355 previously (Zhao et al., 2015).

356

357 **FITC-albumin and 10 kD dextran uptake assays**

358 Nephrocyte functional assays were performed ex vivo at room temperature, following a
359 previously described method (Wen et al., 2020) with minor changes. *Drosophila* females were
360 dissected in Schneider's Drosophila Medium (Thermo Fisher Scientific, MA), then incubated
361 in a 10 kD Texas Red-dextran solution (0.05 mg/mL; D1828, Thermo Fisher Scientific, MA) in
362 Schneider's Drosophila Medium (Thermo Fisher Scientific, MA) for 20 min, or a FITC-albumin
363 solution (10 mM; Sigma, A9771) in Schneider's Drosophila Medium (Thermo Fisher Scientific,
364 MA) for 5 min. The specimens were washed in artificial hemolymph twice, followed by fixation
365 in 4% paraformaldehyde (PFA) for 60 min. Then the fixed specimens were washed thrice for
366 5 min in 1x phosphate buffered saline (1xPBS; pH 7.4) and mounted using Vectashield
367 mounting medium (H-1000, Vector Laboratories, CA). FITC-albumin and 10 kD dextran
368 specimens were imaged using a ZEISS LSM900 confocal microscope with ZEISS Zen
369 acquisition software (blue edition; version 3.0) using a 20× Plan-Apochromat 0.8 N.A. air
370 objective (ZEISS, Oberkochen, Germany). For quantitative comparison of fluorescence
371 intensities, setting for the control condition were chosen to avoid oversaturation (using Range
372 Indicator in ZEN blue; limiting the observed red dots to avoid oversaturation), then applied
373 across the images for all samples/conditions within the assay. The fluorescence intensity of
374 FITC-albumin and 10 kD dextran nephrocytes was determined using Fiji software (Image J

375 (Schneider et al., 2012) , version 2.9.0/1.53t; National Institutes of Health, Bethesda, MD). For
376 quantitation, for each genotype, the relative fluorescence intensity of 30 nephrocytes from 6
377 female flies (5 nephrocytes/fly) was analyzed.
378
379 **Immunochemistry**
380 Immunostaining was performed as previously reported (Zhao et al., 2022) with minor changes.
381 Flies were briefly rinsed in 95% ethanol and dissected in 1xPBS at room temperature.
382 Specimens were incubated in primary antibodies overnight at 4 °C. The incubations in
383 secondary antibodies were performed either overnight at 4 °C or for 2 hours at room
384 temperature. The following antibodies were used: chicken anti-GFP (1:1,000; ab13970,
385 RRID:AB_300798, Abcam, Cambridge, UK), mouse monoclonal anti-Pyd (1:100;
386 RRID:AB_2618043, Developmental Studies Hybridoma Bank, IA), goat anti-mouse Alexa fluor
387 488 (1:500; A11029, RRID:AB_2534088, Invitrogen, Eugene, OR), and goat anti-chicken
388 Alexa fluor 488 (1:500; A11039, AB_2534096, Invitrogen, Eugene, OR). DAPI (0.5 mg/ml in
389 PBST (0.2% Triton-x 100 in 1xPBS); D1306, Thermo Fisher Scientific, MA) was used to
390 visualize the nuclei. The nephrocytes were imaged using a ZEISS LSM900 confocal
391 microscope (under airyscan mode for Pyd images) with ZEISS ZEN acquisition software (blue
392 edition; version 3.0) and a 63× Plan-Apochromat 1.4 N.A. oil objective (ZEISS, Oberkochen,
393 Germany). For quantitative comparison of fluorescence intensities, setting for the control
394 condition were chosen to avoid oversaturation (using Range Indicator in ZEN blue; limiting the
395 observed red dots to avoid oversaturation), then applied across the images for all
396 samples/conditions within the assay. Image J (Schneider et al., 2012) was used for image
397 processing (version 2.9.0/1.53t; National Institutes of Health, Bethesda, MD). Typically, six
398 flies were imaged per condition, representative images for each are displayed in the figures.
399
400 **Transmission electron microscopy (TEM)**
401 TEM was performed using standardized procedures. In brief, female adults (7-days-old) were
402 dissected in Schneider's Drosophila Medium (Thermo Fisher Scientific, MA). The heart tube
403 and the attached nephrocytes were dissected, removed, and fixed using Sorensen phosphate
404 buffer (2% PFA, 2.5% EM grade glutaraldehyde, 2mM $CaCl_2$, 0.1 M NaOH; provided by the
405 Electron Microscopy Core Imaging Facility at the Center for Innovative Biomedical Resources
406 (CIBR), University of Maryland School of Medicine, MD). The processed specimens were
407 imaged using a Philips CM100 TEM, carried out at the Electron Microscopy Core Imaging
408 Facility at the Center for Innovative Biomedical Resources (CIBR) (University of Maryland
409 School of Medicine, MD). The LC-LC distances were measured using the Straight Line tool in
410 Fiji (Image J (Schneider et al., 2012) , version 2.9.0/1.53t; National Institutes of Health,
411 Bethesda, MD) to connect two adjacent lacuna channels (LCs); a straight line was drawn from

412 the middle of the first LC to the middle of the sixth LC, covering five LC-LC intervals on a TEM
413 image, then the measure function was used to obtain the distance value. In total 60 LC-LC
414 distances were measure per condition in 10 nephrocytes from six 7-day-old female flies. The
415 presence of a dark electron dense structure in the vacuoles was manually determined and
416 counted in images obtained from 12 nephrocytes for NFD and 29 nephrocytes from HFD from
417 six 7-day-old female flies.
418
419 **Tissue mosaic analysis**
420 Flp-out clone (Struhl and Basler, 1993) induction was performed as previously described
421 (Duan et al., 2020). In brief, female virgins of *hs-Flp*^{122}; UAS-*Flp*^{JD1}/CyO, *Act-GFP*^{JMR1};
422 *Act5C>CD2>Gal4*^{S}, UAS-*mCD8-GFP*^{LL6}/TM6b (Zhao et al., 2015) were crossed with UAS-
423 *hop.Tum* males. The embryos were collected for 24 hours. First instar larvae (24 hrs after
424 embryo collection) received a 10 min heat shock in a 37°C water bath to induce the mosaic
425 clones. After the heat shock, the larvae were maintained at 25°C. One-day-old female adults
426 were subjected to the 10 kD dextran functional assay (described above). The GFP-positive
427 nephrocyte clones and their neighboring nephrocytes were analyzed.
428
429 **Methotrexate treatment**
430 Flies were dissected as described for the nephrocyte functional assays. The dorsal cuticle
431 (with nephrocytes) was transferred to methotrexate solution (10 μM; 06563, Sigma-Aldrich,
432 MO) in Schneider's Drosophila Medium (Thermo Fisher Scientific, MA) and incubated at room
433 temperature for 60 min. The specimens were rinsed with Schneider's Drosophila Medium
434 (Thermo Fisher Scientific, MA), then subjected to a functional assay or fixed in 4% PFA for
435 immunochemistry.
436
437 **Data analyses and figure preparation**
438 Image J (Schneider et al., 2012) (version 2.9.0/1.53t; National Institutes of Health, Bethesda,
439 MD) was used to process the raw data of confocal images and to measure the relative
440 fluorescence intensity. The data sets were tested for normality using the Shapiro-Wilk test and
441 plotted using GraphPad Prism9 software (version 9.5.1). Normally distributed data were
442 analyzed by the two-tailed Student's t-test, or by two-way ANOVA with Sidak correction. Non-
443 normally distributed data were analyzed by Mann-Whitney U test. $P < 0.05$ was considered
444 significant. The figures were arranged using Adobe Illustrator software (version 2022 26.2.1).
445
446
447 **ACKNOWLEDGMENTS**
448

We thank the Bloomington Drosophila Stock Center (BDSC) based at Indiana University (Bloomington, IN), the Vienna Drosophila Resource Center (VDRC) based at Vienna BioCenter (Vienna, Austria), Prof. Norbert Perrimon (Harvard Medical School, Boston, MA; Howard Hughes Medical Institute, Boston, MA), and Prof. Ylva Engström (Stockholm University, Stockholm, Sweden) for sharing *Drosophila* stocks; and the Developmental Studies Hybridoma Bank (DSHB) based at the University of Iowa (Iowa City, IA) for the providing the antibodies. Finally, we thank the Electron Microscopy Core Imaging Facility at the Center for Innovative Biomedical Resources (CIBR) (University of Maryland School of Medicine, MD, USA) for their support in TEM image acquisition.

FUNDING

This work was support by National Institutes of Health grants R01-DK098410 (Z.H.).

DATA AVAILABILITY

All relevant data can be found within the article and its supplementary information. Requests for resources and reagents related to this manuscript should be directed to and will be fulfilled by the lead contact, Dr. Zhe Han (zhan@som.umaryland.edu).

AUTHOR CONTRIBUTIONS

Z.H. and Y.Z. designed the study; Y.Z. and J.D. carried out the experiments; Y.Z., J.D., J.vdL., and Z.H. analyzed and interpreted the data; Y.Z. prepared the figures; Y.Z., J.vdL., and Z.H. drafted and revised the manuscript; the manuscript has been critically reviewed and the final version approved by all authors. **ORCIDs:** Yunpo Zhao (0000-0002-7942-3406); Jianli Duan (0000-0001-7347-4774); Joyce van de Leemput (0000-0003-1903-7295); Zhe Han (0000-0002-5177-7798)

DISCLOSURES

The authors declare no competing interests.

REFERENCES

Alizadeh S, Esmaeili H, Alizadeh M, Daneshzad E, Sharifi L, Radfar H, Radaei MK. 2019. Metabolic phenotypes of obese, overweight, and normal weight individuals and risk of chronic kidney disease: a systematic review and meta-analysis. *Arch Endocrinol Metab* **63**:427–437.

Altunkaynak ME, Ozbek E, Altunkaynak BZ, Can I, Unal D, Unal B. 2008. The effects of high-fat diet on the renal structure and morphometric parametric of kidneys in rats. *J Anat* **212**:845–852.

Ashraf S, Gee HY, Woerner S, Xie LX, Vega-Warner V, Lovric S, Fang H, Song X, Cattran DC, Avila-Casado C, Paterson AD, Nitschké P, Bole-Feysot C, Cochat P, Esteve-Rudd J, Haberberger B, Allen SJ, Zhou W, Airik R, Otto EA, Barua M, Al-Hamed MH, Kari JA, Evans J, Bierzynska A, Saleem MA, Böckenhauer D, Kleta R, El Desoky S, Hacihamdioglu DO, Gok F, Washburn J, Wiggins RC, Choi M, Lifton RP, Levy S, Han Z, Salviati L, Prokisch H, Williams DS, Pollak M, Clarke CF, Pei Y, Antignac C, Hildebrandt F. 2013. ADCK4 mutations promote steroid-resistant nephrotic syndrome through CoQ10 biosynthesis disruption. *J Clin Invest* **123**:5179–5189.

Banerjee D, Winocour P, Chowdhury TA, De P, Wahba M, Montero R, Fogarty D, Frankel AH, Karalliedde J, Mark PB, Patel DC, Pokrajac A, Sharif A, Zac-Varghese S, Bain S, Dasgupta I, Association of British Clinical Diabetologists and The Renal Association. 2022. Management of hypertension and renin-angiotensin-aldosterone system blockade in adults with diabetic kidney disease: Association of British Clinical Diabetologists and the Renal Association UK guideline update 2021. *BMC Nephrol* **23**:9.

Banes AK, Shaw S, Jenkins J, Redd H, Amiri F, Pollock DM, Marrero MB. 2004. Angiotensin II blockade prevents hyperglycemia-induced activation of JAK and STAT proteins in diabetic rat kidney glomeruli. *Am J Physiol Renal Physiol* **286**:F653-9.

Berthier CC, Zhang H, Schin M, Henger A, Nelson RG, Yee B, Boucherot A, Neusser MA, Cohen CD, Carter-Su C, Argetsinger LS, Rastaldi MP, Brosius FC, Kretzler M. 2009. Enhanced Expression of Janus Kinase–Signal Transducer and Activator of Transcription Pathway Members in Human Diabetic Nephropathy. *Diabetes* **58**:469–477.

Berthoux F, Mariat C, Maillard N. 2013. Overweight/obesity revisited as a predictive risk factor in primary IgA nephropathy. *Nephrol Dial Transplant* **28 Suppl 4**:iv160-6.

Bierzynska A, Bull K, Miellet S, Dean P, Neal C, Colby E, McCarthy HJ, Hegde S, Sinha MD, Bugarin Diz C, Stirrups K, Megy K, Mapeta R, Penkett C, Marsh S, Forrester N, Afzal M, Stark H, BioResource N, Williams M, Welsh GI, Koziell AB, Hartley PS, Saleem MA. 2022. Exploring the relevance of NUP93 variants in steroid-resistant nephrotic syndrome using next generation sequencing and a fly kidney model. *Pediatr Nephrol* **37**:2643–2656.

Bonnet F, Deprele C, Sassolas A, Moulin P, Alamartine E, Berthezène F, Berthoux F. 2001. Excessive body weight as a new independent risk factor for clinical and pathological progression in primary IgA nephritis. *Am J Kidney Dis* **37**:720–727.

Brosius FC, Tuttle KR, Kretzler M. 2016. JAK inhibition in the treatment of diabetic kidney disease. *Diabetologia* **59**:1624–1627.

Brown S, Hu N, Hombría JC. 2001. Identification of the first invertebrate interleukin JAK/STAT receptor, the Drosophila gene domeless. *Curr Biol* **11**:1700–1705.

Cai M-Y, Jiang X-S, Wei Y-X, Wen R-Z, Du X-G. 2024. Role of TFEB-autophagy lysosomal pathway in palmitic acid induced renal tubular epithelial cell injury. *Biochem Biophys Res Commun* **696**:149472.

Callus BA, Mathey-Prevot B. 2002. SOCS36E, a novel Drosophila SOCS protein, suppresses JAK/STAT and EGF-R signalling in the imaginal wing disc. *Oncogene* **21**:4812–4821.

539 Considine RV, Sinha MK, Heiman ML, Kriauciunas A, Stephens TW, Nyce MR, Ohannesian
540 JP, Marco CC, McKee LJ, Bauer TL. 1996. Serum immunoreactive-leptin
541 concentrations in normal-weight and obese humans. *N Engl J Med* **334**:292–295.
542 Coresh J. 2017. Update on the Burden of CKD. *J Am Soc Nephrol* **28**:1020–1022.
543 Curran SP, Famure O, Li Y, Kim SJ. 2014. Increased recipient body mass index is associated
544 with acute rejection and other adverse outcomes after kidney transplantation.
545 *Transplantation* **97**:64–70.
546 Deji N, Kume S, Araki S-I, Soumura M, Sugimoto T, Isshiki K, Chin-Kanasaki M, Sakaguchi
547 M, Koya D, Haneda M, Kashiwagi A, Uzu T. 2009. Structural and functional changes
548 in the kidneys of high-fat diet-induced obese mice. *American Journal of Physiology-*
549 *Renal Physiology* **296**:F118–F126.
550 Duan J, Zhao Y, Li H, Habernig L, Gordon MD, Miao X, Engstrom Y, Buttner S. 2020. Bab2
551 Functions as an Ecdysone-Responsive Transcriptional Repressor during Drosophila
552 Development. *Cell Rep* **32**:107972.
553 Ekas LA, Baeg G-H, Flaherty MS, Ayala-Camargo A, Bach EA. 2006. JAK/STAT signaling
554 promotes regional specification by negatively regulating wingless expression in
555 Drosophila. *Development* **133**:4721–4729.
556 Fu Y, Zhu J-Y, Richman A, Zhao Z, Zhang F, Ray PE, Han Z. 2017. A Drosophila model
557 system to assess the function of human monogenic podocyte mutations that cause
558 nephrotic syndrome. *Hum Mol Genet* **26**:768–780.
559 GBD Chronic Kidney Disease Collaboration. 2020. Global, regional, and national burden of
560 chronic kidney disease, 1990-2017: a systematic analysis for the Global Burden of
561 Disease Study 2017. *Lancet* **395**:709–733.
562 Gee HY, Saisawat P, Ashraf S, Hurd TW, Vega-Warner V, Fang H, Beck BB, Gribouval O,
563 Zhou W, Diaz KA, Natarajan S, Wiggins RC, Lovric S, Chernin G, Schoeb DS, Ovunc
564 B, Frishberg Y, Soliman NA, Fathy HM, Goebel H, Hoefele J, Weber LT, Innis JW, Faul
565 C, Han Z, Washburn J, Antignac C, Levy S, Otto EA, Hildebrandt F. 2013. ARHGDIA
566 mutations cause nephrotic syndrome via defective RHO GTPase signaling. *J Clin*
567 *Invest* **123**:3243–3253.
568 Gee HY, Zhang F, Ashraf S, Kohl S, Sadowski CE, Vega-Warner V, Zhou W, Lovric S, Fang
569 H, Nettleton M, Zhu J-Y, Hoefele J, Weber LT, Podracka L, Boor A, Fehrenbach H,
570 Innis JW, Washburn J, Levy S, Lifton RP, Otto EA, Han Z, Hildebrandt F. 2015. KANK
571 deficiency leads to podocyte dysfunction and nephrotic syndrome. *J Clin Invest*
572 **125**:2375–2384.
573 Gonçalves S, Patat J, Guida MC, Lachaussée N, Arrondel C, Helmstädter M, Boyer O,
574 Gribouval O, Gubler M-C, Mollet G, Rio M, Charbit M, Bole-Feysot C, Nitschke P,
575 Huber TB, Wheeler PG, Haynes D, Juusola J, Billette de Villemeur T, Nava C, Afenjar
576 A, Keren B, Bodmer R, Antignac C, Simons M. 2018. A homozygous KAT2B variant
577 modulates the clinical phenotype of ADD3 deficiency in humans and flies. *PLoS Genet*
578 **14**:e1007386.
579 Ha S, Yang Y, Kim BM, Kim J, Son M, Kim D, Yu HS, Im D-S, Chung HY, Chung KW. 2022.
580 Activation of PAR2 promotes high-fat diet-induced renal injury by inducing oxidative
581 stress and inflammation. *Biochim Biophys Acta Mol Basis Dis* **1868**:166474.
582 Hao J, Zhang Y-J, Lv X, Xu N, Liu Q-J, Zhao S, Feng X-J, Xing L-L, Kang P-P, Li G-Y, Liu S-
583 X. 2013. IFN-γ induces lipogenesis in mouse mesangial cells via the JAK2/STAT1
584 pathway. *Am J Physiol Cell Physiol* **304**:C760-7.
585 Harrison DA, Binari R, Nahreini TS, Gilman M, Perrimon N. 1995. Activation of a Drosophila
586 Janus kinase (JAK) causes hematopoietic neoplasia and developmental defects.
587 *EMBO J* **14**:2857–2865.
588 Heimbürger O, Lönnqvist F, Danielsson A, Nordenström J, Stenvinkel P. 1997. Serum
589 immunoreactive leptin concentration and its relation to the body fat content in chronic
590 renal failure. *J Am Soc Nephrol* **8**:1423–1430.
591 Herman-Edelstein M, Scherzer P, Tobar A, Levi M, Gafter U. 2014. Altered renal lipid
592 metabolism and renal lipid accumulation in human diabetic nephropathy. *J Lipid Res*
593 **55**:561–572.

Hermle T, Braun DA, Helmstädter M, Huber TB, Hildebrandt F. 2017. Modeling Monogenic Human Nephrotic Syndrome in the Drosophila Garland Cell Nephrocyte. *J Am Soc Nephrol* **28**:1521–1533.

Hermle T, Schneider R, Schapiro D, Braun DA, van der Ven AT, Warejko JK, Daga A, Widmeier E, Nakayama M, Jobst-Schwan T, Majmundar AJ, Ashraf S, Rao J, Finn LS, Tasic V, Hernandez JD, Bagga A, Jalalah SM, El Desoky S, Kari JA, Laricchia KM, Lek M, Rehm HL, MacArthur DG, Mane S, Lifton RP, Shril S, Hildebrandt F. 2018. GAPVD1 and ANKFY1 Mutations Implicate RAB5 Regulation in Nephrotic Syndrome. *J Am Soc Nephrol* **29**:2123–2138.

Hombria JC, Brown S, Hader S, Zeidler MP. 2005. Characterisation of Upd2, a Drosophila JAK/STAT pathway ligand. *Dev Biol* **288**:420–433.

Hsu C-Y, McCulloch CE, Iribarren C, Darbinian J, Go AS. 2006. Body mass index and risk for end-stage renal disease. *Ann Intern Med* **144**:21–28.

Huo R, Huang X, Yang Y, Lin J. 2023. Potential Use of Janus Kinase Inhibitors in the Treatment of Systemic Lupus Erythematosus. *J Inflamm Res* **16**:1471–1478.

Jiang T, Wang Z, Proctor G, Moskowitz S, Liebman SE, Rogers T, Lucia MS, Li J, Levi M. 2005. Diet-induced obesity in C57BL/6J mice causes increased renal lipid accumulation and glomerulosclerosis via a sterol regulatory element-binding protein-1c-dependent pathway. *J Biol Chem* **280**:32317–32325.

Jiang Z, Wang Y, Zhao X, Cui H, Han M, Ren X, Gang X, Wang G. 2023. Obesity and chronic kidney disease. *Am J Physiol Endocrinol Metab* **324**:E24–E41.

Karsten P, Häder S, Zeidler MP. 2002. Cloning and expression of Drosophila SOCS36E and its potential regulation by the JAK/STAT pathway. *Mech Dev* **117**:343–346.

Kimmelstiel P, Wilson C. 1936. Intercapillary lesions in the glomeruli of the kidney. *Am J Pathol* **12**:83-98.7.

Kuwahara S, Hosojima M, Kaneko R, Aoki H, Nakano D, Sasagawa T, Kabasawa H, Kaseda R, Yasukawa R, Ishikawa T, Suzuki A, Sato H, Kageyama S, Tanaka T, Kitamura N, Narita I, Komatsu M, Nishiyama A, Saito A. 2016. Megalin-Mediated Tubuloglomerular Alterations in High-Fat Diet-Induced Kidney Disease. *J Am Soc Nephrol* **27**:1996–2008.

Li C, Lin Y, Luo R, Chen S, Wang F, Zheng P, Levi M, Yang T, Wang W. 2016. Intrarenal renin-angiotensin system mediates fatty acid-induced ER stress in the kidney. *Am J Physiol Renal Physiol* **310**:F351-63.

Li H, Li M, Liu P, Wang Y, Zhang H, Li Hongbin, Yang S, Song Y, Yin Y, Gao L, Cheng S, Cai J, Tian G. 2016. Telmisartan Ameliorates Nephropathy in Metabolic Syndrome by Reducing Leptin Release From Perirenal Adipose Tissue. *Hypertension* **68**:478–490.

Liu Y-H, Jakobsen JS, Valentin G, Amarantos I, Gilmour DT, Furlong EEM. 2009. A systematic analysis of Tinman function reveals Eya and JAK-STAT signaling as essential regulators of muscle development. *Dev Cell* **16**:280–291.

Lu J, Bankovic-Calic N, Ogborn M, Saboorian MH, Aukema HM. 2003. Detrimental Effects of a High Fat Diet in Early Renal Injury Are Ameliorated by Fish Oil in Han:SPRD-cy Rats. *J Nutr* **133**:180–186.

Lubojemska A, Stefana MI, Sorge S, Bailey AP, Lampe L, Yoshimura A, Burrell A, Collinson L, Gould AP. 2021. Adipose triglyceride lipase protects renal cell endocytosis in a Drosophila dietary model of chronic kidney disease. *PLoS Biol* **19**:e3001230.

McGuire SE, Mao Z, Davis RL. 2004. Spatiotemporal gene expression targeting with the TARGET and gene-switch systems in Drosophila. *Sci STKE* **2004**:l6.

Milosavljevic J, Lempicki C, Lang K, Heinkele H, Kampf LL, Leroy C, Chen M, Gerstner L, Spitz D, Wang M, Knob AU, Kayser S, Helmstädter M, Walz G, Pollak MR, Hermle T. 2022. Nephrotic Syndrome Gene TBC1D8B Is Required for Endosomal Maturation and Nephrin Endocytosis in Drosophila. *J Am Soc Nephrol* **33**:2174–2193.

Moorhead JF, Chan MK, El-Nahas M, Varghese Z. 1982. Lipid nephrotoxicity in chronic progressive glomerular and tubulo-interstitial disease. *Lancet* **2**:1309–1311.

Odenthal J, Dittrich S, Ludwig V, Merz T, Reitmeier K, Reusch B, Höhne M, Cosgun ZC, Hohenadel M, Putnik J, Göbel H, Rinschen MM, Altmüller J, Koehler S, Schermer B,

Benzing T, Beck BB, Brinkkötter PT, Habbig S, Bartram MP. 2023. Modeling of ACTN4-Based Podocytopathy Using Drosophila Nephrocytes. *Kidney Int Rep* **8**:317–329.

Paul MS, Duncan AR, Genetti CA, Pan H, Jackson A, Grant PE, Shi J, Pinelli M, Brunetti-Pierri N, Garza-Flores A, Shahani D, Saneto RP, Zampino G, Leoni C, Agolini E, Novelli A, Blümlein U, Haack TB, Heinritz W, Matzker E, Alhaddad B, Abou Jamra R, Bartolomaeus T, AlHamdan S, Carapito R, Isidor B, Bahram S, Ritter A, Izumi K, Shakked BP, Barel O, Ben Zeev B, Begtrup A, Carere DA, Mullegama SV, Palculict TB, Calame DG, Schwan K, Aycinena ARP, Traberg R, Genomics England Research Consortium, Douzgou S, Pirt H, Ismayilova N, Banka S, Chao H-T, Agrawal PB. 2023. Rare EIF4A2 variants are associated with a neurodevelopmental disorder characterized by intellectual disability, hypotonia, and epilepsy. *Am J Hum Genet* **110**:120–145.

Rajan A, Housden BE, Wirtz-Peitz F, Holderbaum L, Perrimon N. 2017. A Mechanism Coupling Systemic Energy Sensing to Adipokine Secretion. *Dev Cell* **43**:83-98 e6.

Rajan A, Perrimon N. 2012. Drosophila cytokine unpaired 2 regulates physiological homeostasis by remotely controlling insulin secretion. *Cell* **151**:123–137.

Rangel Silvares R, Nunes Goulart da Silva Pereira E, Eduardo Ilaquita Flores E, Lino Rodrigues K, Ribeiro Silva A, Gonçalves-de-Albuquerque CF, Daliry A. 2019. High-fat diet-induced kidney alterations in rats with metabolic syndrome: endothelial dysfunction and decreased antioxidant defense. *Diabetes Metab Syndr Obes* **12**:1773–1781.

Recasens-Alvarez C, Ferreira A, Milán M. 2017. JAK/STAT controls organ size and fate specification by regulating morphogen production and signalling. *Nat Commun* **8**:13815.

Ruggiero C, Ehrenshaft M, Cleland E, Stadler K. 2011. High-fat diet induces an initial adaptation of mitochondrial bioenergetics in the kidney despite evident oxidative stress and mitochondrial ROS production. *American Journal of Physiology-Endocrinology and Metabolism* **300**:E1047–E1058.

Sánchez-Navarro A, Martínez-Rojas MÁ, Caldiño-Bohn RI, Pérez-Villalva R, Zambrano E, Castro-Rodríguez DC, Bobadilla NA. 2021. Early triggers of moderately high-fat diet-induced kidney damage. *Physiol Rep* **9**:e14937.

Schneider CA, Rasband WS, Eliceiri KW. 2012. NIH Image to ImageJ: 25 years of image analysis. *Nat Methods* **9**:671–675.

Serrano E, Shenoy P, Martinez Cantarin MP. 2023. Adipose tissue metabolic changes in chronic kidney disease. *Immunometabolism (Cobham)* **5**:e00023.

Struhl G, Basler K. 1993. Organizing activity of wingless protein in Drosophila. *Cell* **72**:527–540.

Sun Y, Ge X, Li Xue, He J, Wei X, Du J, Sun J, Li Xin, Xun Z, Liu W, Zhang H, Wang Z-Y, Li YC. 2020. High-fat diet promotes renal injury by inducing oxidative stress and mitochondrial dysfunction. *Cell Death Dis* **11**:1–14.

Szeto HH, Liu S, Soong Y, Alam N, Prusky GT, Seshan SV. 2016. Protection of mitochondria prevents high-fat diet-induced glomerulopathy and proximal tubular injury. *Kidney Int* **90**:997–1011.

Thomas S, Fisher KH, Snowden JA, Danson SJ, Brown S, Zeidler MP. 2015. Methotrexate Is a JAK/STAT Pathway Inhibitor. *PLoS One* **10**:e0130078.

Tsuboi N, Koike K, Hirano K, Utsunomiya Y, Kawamura T, Hosoya T. 2013. Clinical features and long-term renal outcomes of Japanese patients with obesity-related glomerulopathy. *Clin Exp Nephrol* **17**:379–385.

Tuttle KR, Brosius FC 3rd, Adler SG, Kretzler M, Mehta RL, Tumlin JA, Tanaka Y, Haneda M, Liu J, Silk ME, Cardillo TE, Duffin KL, Haas JV, Macias WL, Nunes FP, Janes JM. 2018. JAK1/JAK2 inhibition by baricitinib in diabetic kidney disease: results from a Phase 2 randomized controlled clinical trial. *Nephrol Dial Transplant* **33**:1950–1959.

US Department of Health and Human Services, Centers for Disease Control and Prevention (Atlanta, GA). 2023. Chronic Kidney Disease in the United States, 2023. *Centers for*

Disease Control and Prevention. https://www.cdc.gov/kidneydisease/publications-resources/ckd-national-facts.html

van de Leemput J, Wen P, Han Z. 2022. Using Drosophila Nephrocytes to Understand the Formation and Maintenance of the Podocyte Slit Diaphragm. *Front Cell Dev Biol* **10**:837828.

van der Heijden RA, Bijzet J, Meijers WC, Yakala GK, Kleemann R, Nguyen TQ, de Boer RA, Schalkwijk CG, Hazenberg BPC, Tietge UJF, Heeringa P. 2015. Obesity-induced chronic inflammation in high fat diet challenged C57BL/6J mice is associated with acceleration of age-dependent renal amyloidosis. *Sci Rep* **5**:1–15.

Wang L, Wen P, van de Leemput J, Zhao Z, Han Z. 2021. Slit diaphragm maintenance requires dynamic clathrin-mediated endocytosis facilitated by AP-2, Lap, Aux and Hsc70-4 in nephrocytes. *Cell Biosci* **11**:83.

Weavers H, Prieto-Sánchez S, Grawe F, Garcia-López A, Artero R, Wilsch-Bräuninger M, Ruiz-Gómez M, Skaer H, Denholm B. 2009. The insect nephrocyte is a podocyte-like cell with a filtration slit diaphragm. *Nature* **457**:322–326.

Wen P, Zhang F, Fu Y, Zhu J-Y, Han Z. 2020. Exocyst Genes Are Essential for Recycling Membrane Proteins and Maintaining Slit Diaphragm in Drosophila Nephrocytes. *J Am Soc Nephrol* **31**:1024–1034.

Woodcock KJ, Kierdorf K, Pouchelon CA, Vivancos V, Dionne MS, Geissmann F. 2015. Macrophage-derived upd3 cytokine causes impaired glucose homeostasis and reduced lifespan in Drosophila fed a lipid-rich diet. *Immunity* **42**:133–144.

Yamout H, Lazich I, Bakris GL. 2014. Blood pressure, hypertension, RAAS blockade, and drug therapy in diabetic kidney disease. *Adv Chronic Kidney Dis* **21**:281–286.

Zhang F, Zhao Y, Chao Y, Muir K, Han Z. 2013a. Cubilin and amnionless mediate protein reabsorption in Drosophila nephrocytes. *J Am Soc Nephrol* **24**:209–216.

Zhang F, Zhao Y, Han Z. 2013b. An in vivo functional analysis system for renal gene discovery in Drosophila pericardial nephrocytes. *J Am Soc Nephrol* **24**:191–197.

Zhang H, Nair V, Saha J, Atkins KB, Hodgin JB, Saunders TL, Myers MG Jr, Werner T, Kretzler M, Brosius FC. 2017. Podocyte-specific JAK2 overexpression worsens diabetic kidney disease in mice. *Kidney Int* **92**:909–921.

Zhao F, Zhu J-Y, Richman A, Fu Y, Huang W, Chen N, Pan X, Yi C, Ding X, Wang S, Wang P, Nie X, Huang J, Yang Y, Yu Z, Han Z. 2019. Mutations in NUP160 Are Implicated in Steroid-Resistant Nephrotic Syndrome. *J Am Soc Nephrol* **30**:840–853.

Zhao Y, Cocco C, Domenichini S, Samson ML, Rabinow L. 2015. The IMD innate immunity pathway of Drosophila influences somatic sex determination via regulation of the Doa locus. *Dev Biol* **407**:224–231.

Zhao Y, Khallaf MA, Johansson E, Dzaki N, Bhat S, Alfredsson J, Duan J, Hansson BS, Knaden M, Alenius M. 2022. Hedgehog-mediated gut-taste neuron axis controls sweet perception in Drosophila. *Nat Commun* **13**:7810.

Zhu J-Y, Fu Y, Richman A, Zhao Z, Ray PE, Han Z. 2017. A Personalized Model of COQ2 Nephropathy Rescued by the Wild-Type COQ2 Allele or Dietary Coenzyme Q10 Supplementation. *J Am Soc Nephrol* **28**:2607–2617.

Zhuang S, Shao H, Guo F, Trimble R, Pearce E, Abmayr SM. 2009. Sns and Kirre, the Drosophila orthologs of Nephrin and Neph1, direct adhesion, fusion and formation of a slit diaphragm-like structure in insect nephrocytes. *Development* **136**:2335–2344.

Figure 1

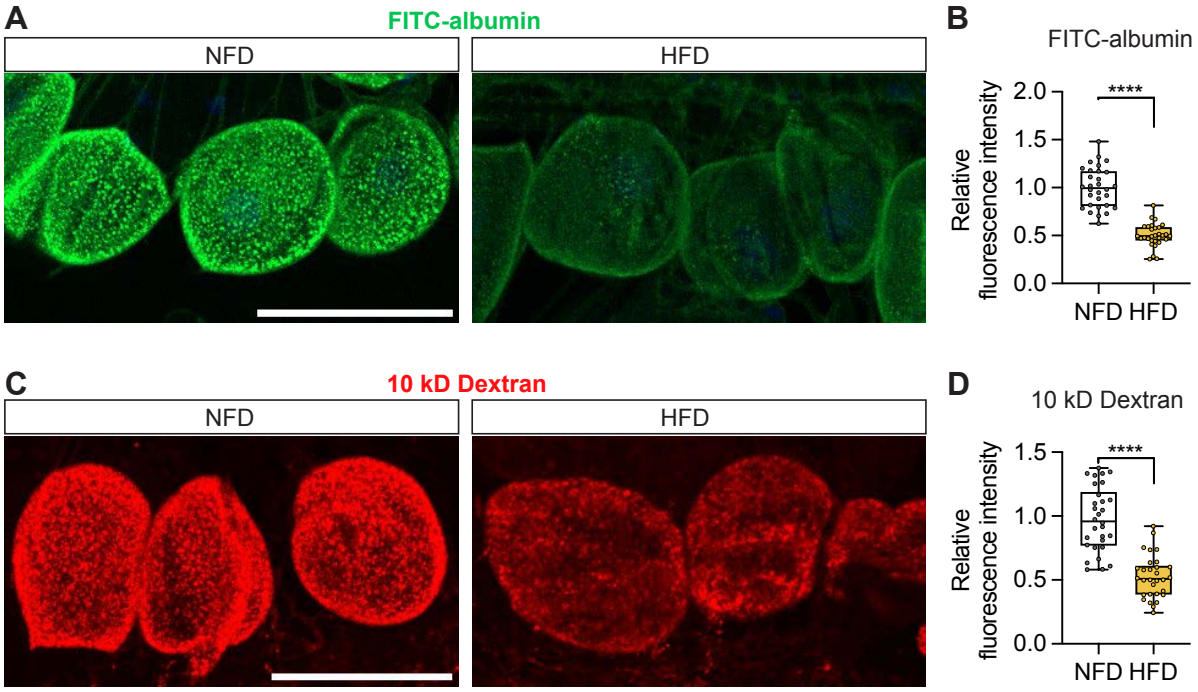
A
FITC-albumin
NFD
HFD
B
FITC-albumin
Relative fluorescence intensity
2.0
1.5
1.0
0.5
0.0
****
NFD HFD
C
10 kD Dextran
NFD
HFD
D
10 kD Dextran
Relative fluorescence intensity
1.5
1.0
0.5
0.0
****
NFD HFD

793 **Figure 1. High-fat diet compromises nephrocyte function**

794 Nephrocytes from control *Drosophila* (w^{1118}, 1-day-old females) fed a regular diet (normal fat
795 diet, NFD) or high-fat diet (NFD supplemented with 14% coconut oil, HFD) for 7 days from
796 eclosion. **(A)** Representative confocal images of nephrocytes show green fluorescence
797 indicative of FITC-albumin uptake. Scale bar: 50 µm. **(B)** Box plot shows the quantitation of
798 the relative fluorescence intensity of FITC-albumin shown in (A); middle line depicts the
799 median and whiskers show Tukey. Statistical analysis was performed with a two-tailed
800 Student's t-test; ****, P<0.0001; n = 30 nephrocytes from six 1-day-old females (5
801 nephrocytes/fly). **(C)** Representative confocal images of *Drosophila* nephrocytes (w^{1118}, 1-day-
802 old females) show red fluorescence indicative of 10 kD dextran uptake. Scale bar: 50 µm. **(D)**
803 Box plot shows the quantitation of the relative fluorescence intensity of 10 kD dextran shown
804 in (C); middle line depicts the median and whiskers show Tukey. Statistical analysis was
805 performed with a two-tailed Student's t-test; ****, P<0.0001; n = 30 nephrocytes from six 1-
806 day-old females (5 nephrocytes/fly).
807
808
809
810
811
812
813
814
815
816
817
818
819
820
821
822
823
824
825
826
827
828
829

Figure 2

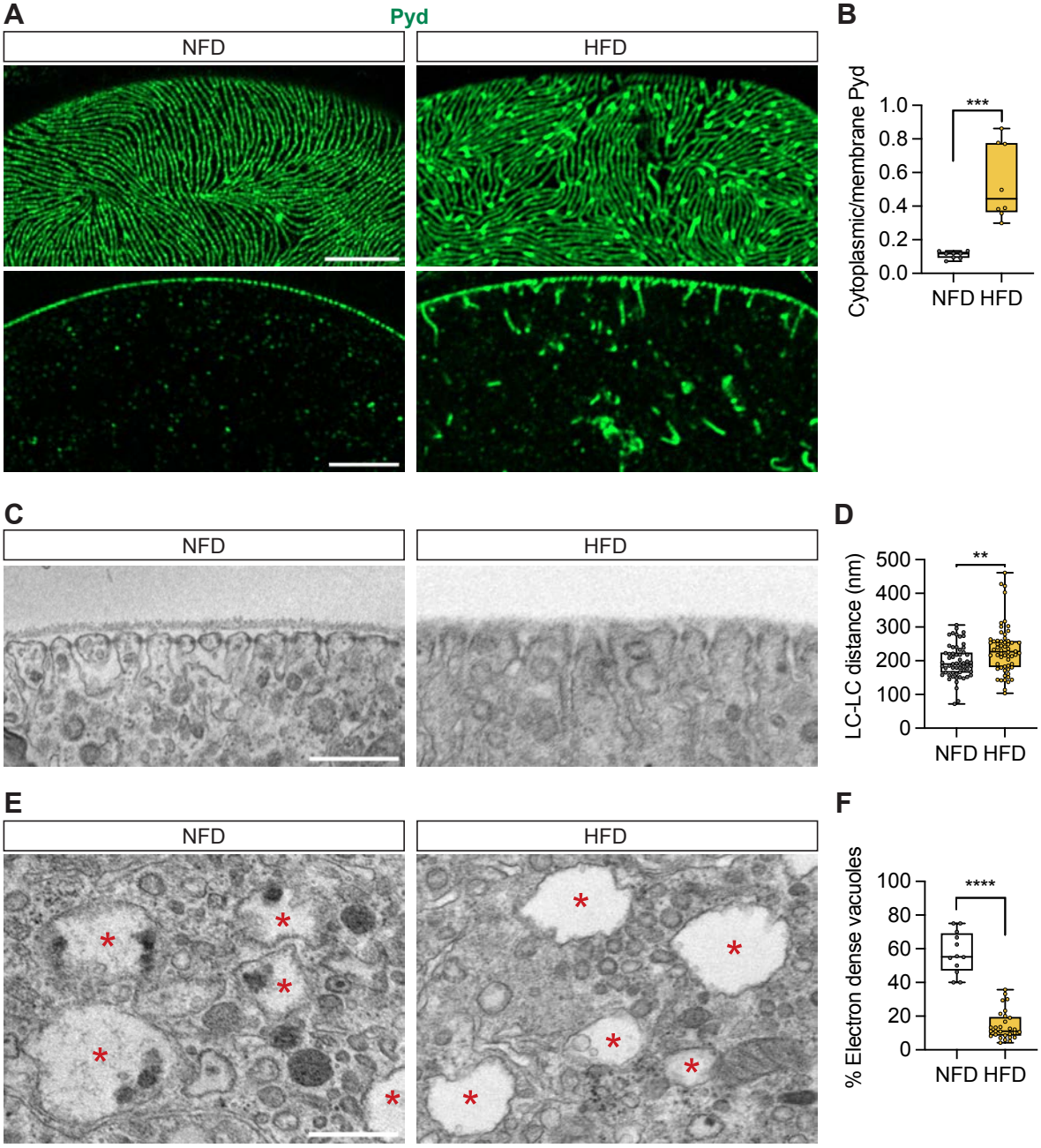
A
Pyd
NFD
HFD
B
Cytoplasmic/membrane Pyd
1.0
0.8
0.6
0.4
0.2
0.0
***
NFD HFD
C
NFD
HFD
D
LC-LC distance (nm)
500
400
300
200
100
0
**
NFD HFD
E
NFD
HFD
F
% Electron dense vacuoles
100
80
60
40
20
0
****
NFD HFD

867 **Figure 2. High-fat diet changes nephrocyte morphology**
868 Nephrocytes from control *Drosophila* (w^{1118}, 7-day-old females) fed a regular diet (normal fat
869 diet, NFD) or high-fat diet (NFD supplemented with 14% coconut oil, HFD). **(A)** Representative
870 confocal images of *Drosophila* nephrocytes immunostained with anti-polychaetoid (Pyd) in
871 green. Upper panels show cortical surface; Scale bar: 5 µm. Lower panels show subcortical
872 regions; Scale bar: 5 µm. **(B)** Quantitation of Pyd protein distribution (cytoplasmic vs
873 membrane); middle line depicts the median and whiskers show Tukey. Statistical analysis was
874 performed with a two-tailed Student's t-test; ***, P<0.001; n = 8 nephrocytes (1 nephrocyte/fly)
875 from 7-day-old female flies. **(C)** Transmission electron microscopy (TEM) images of
876 *Drosophila* nephrocyte (w^{1118}, 7-day-old females) cortical regions. Scale bar: 0.5 µm. **(D)**
877 Quantitation of lacuna channel (LC)-LC distance based on images in (C); middle line depicts
878 the median and whiskers show Tukey. Statistical analysis was performed with a two-tailed
879 Student's t-test; **, P<0.01; n = 60 LC-LC distance measurements obtained in 10 nephrocytes
880 from six 7-day-old female flies for each group. **(E)** TEM images of *Drosophila* nephrocyte
881 (w^{1118}, 7-day-old-females) cytoplasmic regions. Red asterisks indicate large vacuoles. Scale
882 bar: 0.5 µm. **(F)** Quantitation of the vacuoles that contain electron dense structures based on
883 images in (E). The middle line depicts the median and whiskers show Tukey. Statistical
884 analysis was performed with a two-tailed Student's t-test; ****, P<0.0001; n = 12 nephrocytes
885 for NFD and 29 nephrocytes for HFD from six 7-day-old female flies.
886
887
888
889
890
891
892
893
894
895
896
897
898
899
900
901
902
903

Figure 3

A

Human Gene	*Drosophila* Homolog	DIOPT Score	Function
STAT5B	*Stat92E*	13	transcription factor
PTPRQ	*dome*	2	transmembrane receptor
JAK1/JAK2	*hop*	11	non-receptor tyrosine kinase
SOCS4/SOCS5	*Socs36E*	7	negative regulator of JAK-STAT

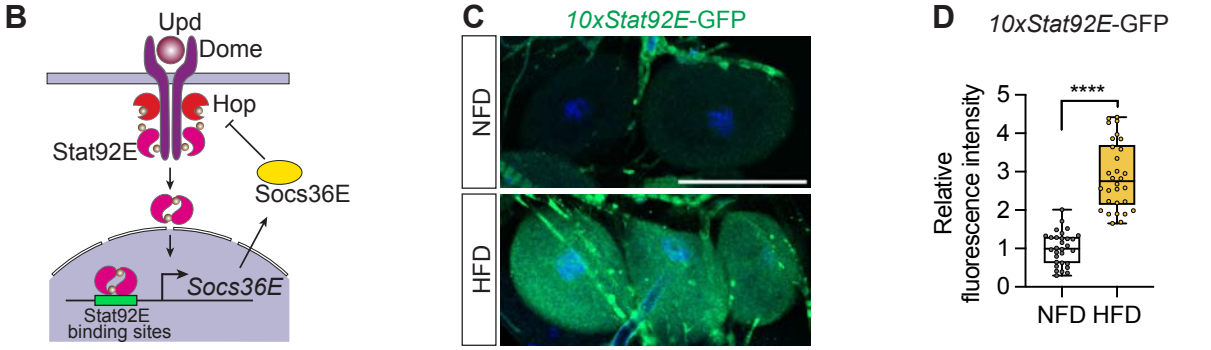

941 **Figure 3. High-fat diet activates the JAK-STAT pathway in nephrocytes**
942 **(A)** Table lists human genes encoding JAK-STAT pathway components, along with their
943 *Drosophila* homologs, the DRSC Integrative Ortholog Prediction Tool (DIOPT) score
944 (maximum score = 15), and their function. **(B)** Graphical representation of the JAK-STAT
945 signaling pathway and interaction between its components. Domeless, Dome; JAK
946 Hopscotch, Hop; Signal-transducer and activator of transcription 92E, Stat92E; Suppressor of
947 cytokine signaling at 36E, Socs36E; Unpaired, Upd. **(C)** Representative confocal images of
948 nephrocytes from control *Drosophila* (*10xStat92E*-GFP, 1-day-old females) fed a regular diet
949 (normal fat diet, NFD) or high-fat diet (NFD supplemented with 14% coconut oil, HFD).
950 *10xStat92E*-GFP is shown in green fluorescence; DAPI (blue) stains DNA to visualize the
951 nucleus. Scale bar: 50 μm. **(D)** Box plot shows the quantitation of the relative fluorescence
952 intensity of *10xStat92E*-GFP based on images in (C); middle line depicts the median and
953 whiskers show Tukey. Statistical analysis was performed with a two-tailed Student's t-test;
954 ****, P<0.0001; n = 30 nephrocytes from six 1-day-old females (5 nephrocytes/fly).
955
956
957
958
959
960
961
962
963
964
965
966
967
968
969
970
971
972
973
974
975
976
977

Figure 4

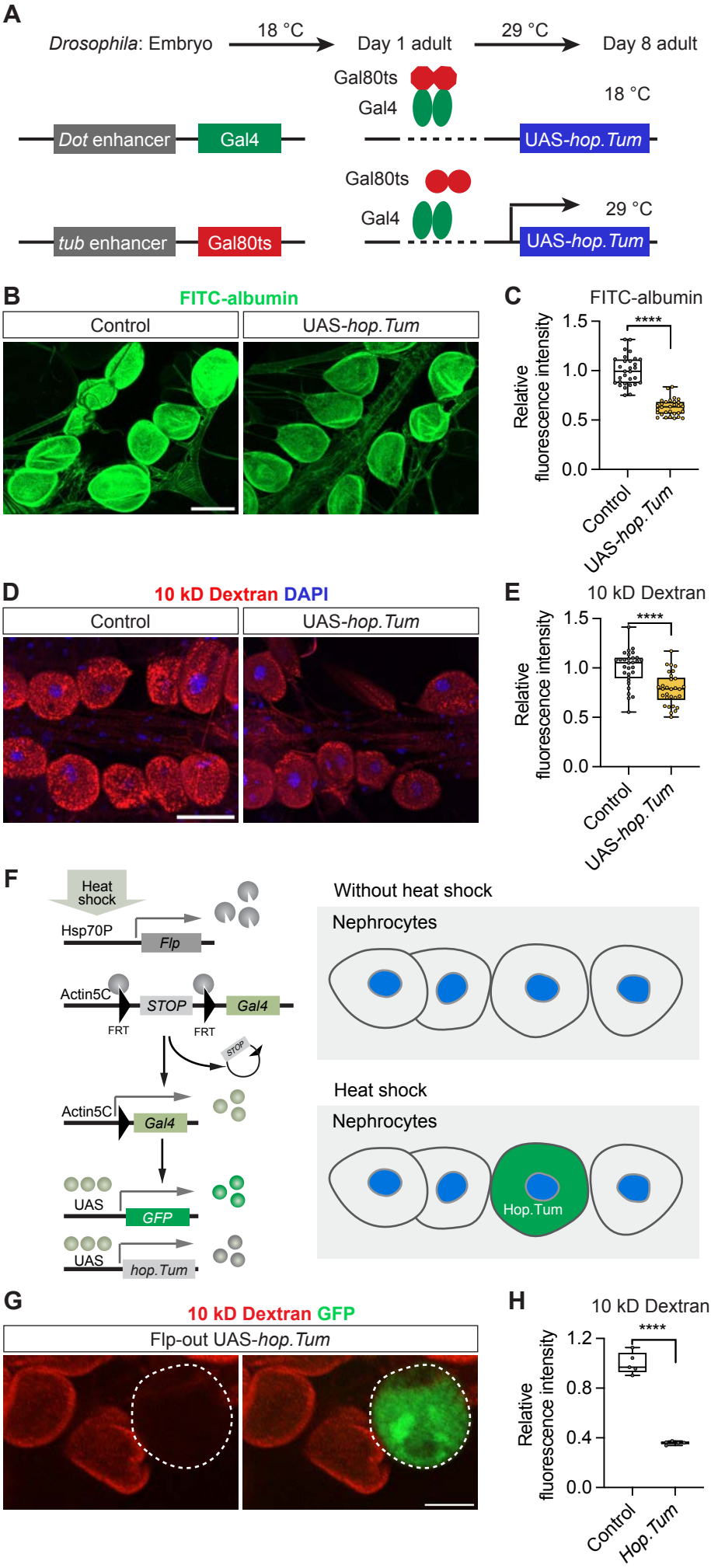
A
Drosophila: Embryo
18 °C
Day 1 adult
29 °C
Day 8 adult
Gal80ts
Gal4
18 °C
Dot enhancer
Gal4
UAS-hop.Tum
Gal80ts
Gal4
29 °C
tub enhancer
Gal80ts
UAS-hop.Tum
B
FITC-albumin
Control
UAS-hop.Tum
C
FITC-albumin
Relative fluorescence intensity
1.5
1.0
0.5
0.0
****
Control
UAS-hop.Tum
D
10 kD Dextran DAPI
Control
UAS-hop.Tum
E
10 kD Dextran
Relative fluorescence intensity
1.5
1.0
0.5
0.0
****
Control
UAS-hop.Tum
F
Heat shock
Hsp70P
Flp
Actin5C
STOP
Gal4
FRT
FRT
STOP
Actin5C
Gal4
UAS
GFP
UAS
hop.Tum
Without heat shock
Nephrocytes
Heat shock
Nephrocytes
Hop.Tum
G
10 kD Dextran GFP
Flp-out UAS-hop.Tum
H
10 kD Dextran
Relative fluorescence intensity
1.2
0.8
0.4
0.0
****
Control
Hop.Tum

1015 **Figure 4. JAK-STAT pathway activation compromises nephrocyte function**
1016 **(A)** Schematic illustration of targeted UAS-*hop.Tum* expression in the nephrocytes;
1017 *hopscotch.Tumorous-lethal*, dominant gain-of-function, constitutively activates JAK-STAT.
1018 Temperature sensitive Gal80ts binds to Gal4 and acts as a negative regulator of the Gal4
1019 transcriptional activator at 18°C. A temperature switch to 29°C releases Gal80ts inhibition as
1020 it can no longer bind Gal4, thus allowing UAS-*hop.Tum* expression driven by Gal4 to occure.
1021 Timeline for temperature switches of the fly at different stages of development have been
1022 indicated. **(B)** Representative confocal images of FITC-albumin fluorescence (green) in
1023 nephrocytes from control flies (*Dot*-Gal4/+; *tub*-Gal80ts/+) and those with activated JAK-STAT
1024 (*Dot*-Gal4/UAS-*hop.Tum*; *tub*-Gal80ts/+). Scale bar: 50 µm. **(C)** Box plot shows the
1025 quantitation of the relative fluorescence intensity of FITC-albumin based on images in (B);
1026 middle line depicts the median and whiskers show Tukey. Statistical analysis was performed
1027 with a two-tailed Student's t-test; ****, P<0.0001; n = 30 from six 1-day-old females (5
1028 nephrocytes/fly). **(D)** Representative confocal images of 10 kD dextran fluorescence (red) in
1029 nephrocytes from control flies (*Dot*-Gal4/+; *tub*-Gal80ts/+) and those with activated JAK-STAT
1030 (*Dot*-Gal4/UAS-*hop.Tum*; *tub*-Gal80ts/+); DAPI (blue) stains DNA to visualize the nucleus.
1031 Scale bar: 50 µm. **(E)** Box plot shows the quantitation of the relative fluorescence intensity of
1032 10 kD dextran uptake based on images in (D); middle line depicts the median and whiskers
1033 show Tukey. Statistical analysis was performed with a two-tailed Student's t-test; ****,
1034 P<0.0001; n = 30 from six 1-day-old females (5 nephrocytes/fly). **(F)** Schematic illustration of
1035 the Flp-out clone strategy to induce UAS-*hop.Tum* expression. Heat shock induces the
1036 expression of Flp recombinase, which excises a stop cassette to initiate Gal4 expression. Gal4
1037 binding to the upstream activation sequences (UAS) drives the expression of GFP (as a
1038 marker for positive Flp-out clones) and UAS-*hop.Tum*. **(G)** Representative confocal images of
1039 10 kD dextran fluorescence (red) in nephrocytes from flies with a GFP labelled Flp-out UAS-
1040 *hop.Tum* clone (*hs-Flp*^{122}/+; UAS-*Flp*^{JD1}/UAS-*hop.Tum*; *Act5C>CD2>Gal4*^{S}, UAS-
1041 *mCD8GFP*^{LL6}/+). **(H)** Box plot shows the quantitation of the relative fluorescence intensity of
1042 10 kD dextran fluorescence uptake based on images in (G); middle line depicts the median
1043 and whiskers show Tukey. Control (neighbor of Flp-out clone; UAS-*hop.Tum* (clone).
1044 Statistical analysis was performed with a two-tailed Student's t-test; ****, P<0.0001; n= 5 from
1045 four 3-day-old females.
1046
1047
1048
1049
1050
1051

Figure 5

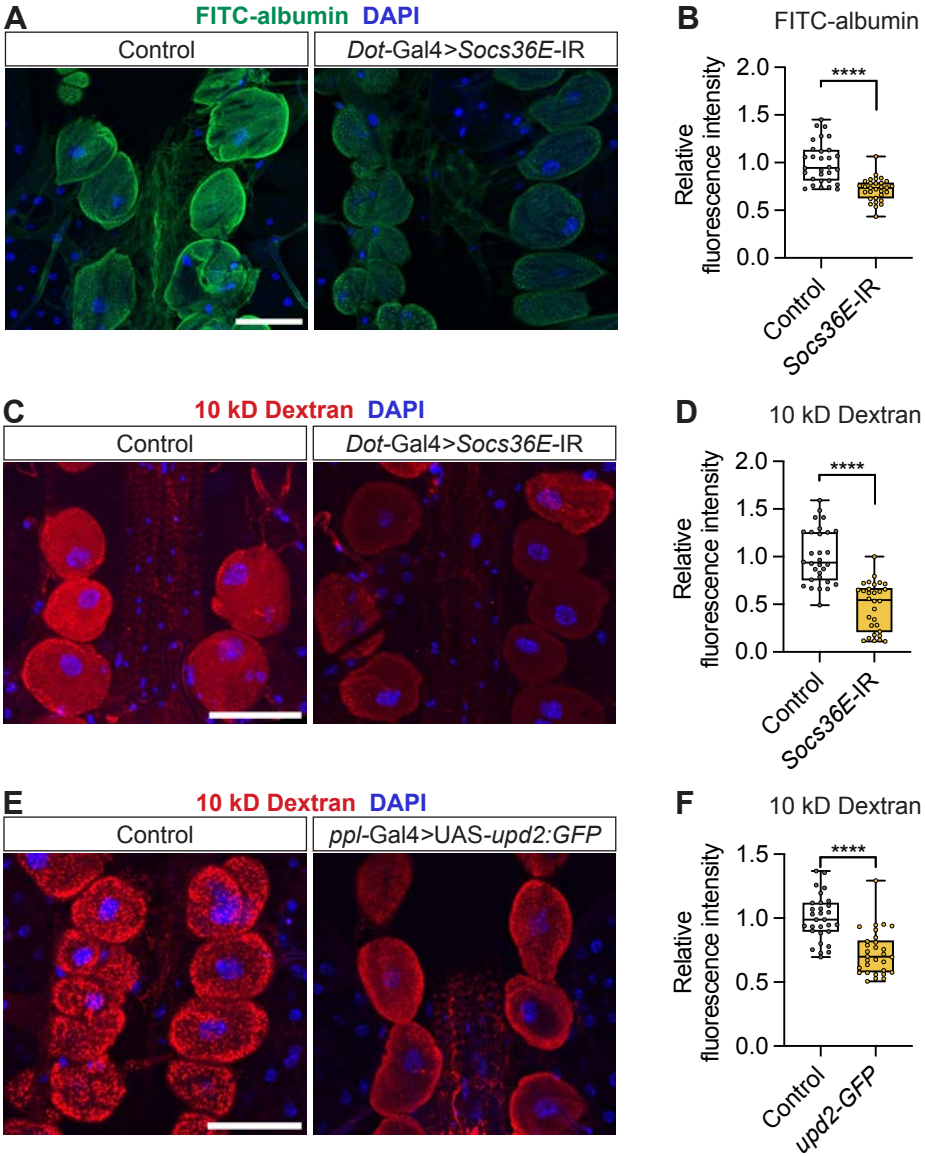
A
FITC-albumin DAPI
Control
Dot-Gal4>Socs36E-IR
B
FITC-albumin
Relative fluorescence intensity
2.0
1.5
1.0
0.5
0.0
****
Control
Socs36E-IR
C
10 kD Dextran DAPI
Control
Dot-Gal4>Socs36E-IR
D
10 kD Dextran
Relative fluorescence intensity
2.0
1.5
1.0
0.5
0.0
****
Control
Socs36E-IR
E
10 kD Dextran DAPI
Control
ppl-Gal4>UAS-upd2:GFP
F
10 kD Dextran
Relative fluorescence intensity
1.5
1.0
0.5
0.0
****
Control
upd2-GFP

1088 **Figure 5. Silencing *Socs36E* in the nephrocytes, or *upd2* overexpression in the fat body,**
1089 **leads to nephrocyte dysfunction**
1090 **(A)** Representative confocal images of FITC-albumin (green) in nephrocytes from control flies
1091 (*Dot*-Gal4/+) and flies with nephrocyte-specific silencing of the Socs36E JAK-STAT inhibitor
1092 (*Dot*-Gal4>*Socs36E*-IR); DAPI (blue) stains DNA to visualize the nucleus. Scale bar: 50 µm.
1093 *Socs36E*, *Suppressor of cytokine signaling at 36E*. **(B)** Box plot shows the quantitation of the
1094 relative fluorescence intensity of FITC-albumin uptake based on images in (A); middle line
1095 depicts the median and whiskers show Tukey. Statistical analysis was performed with a two-
1096 tailed Student's t-test; ****, P<0.0001; n= 30 from six 1-day-old females (5 nephrocytes/fly).
1097 **(C)** Representative confocal images of 10 kD dextran fluorescence (red) in nephrocytes from
1098 control flies (*Dot*-Gal4/+) and flies with nephrocyte-specific silencing of the Socs36E JAK-
1099 STAT inhibitor (*Dot*-Gal4>*Socs36E*-IR); DAPI (blue) stains DNA to visualize the nucleus.
1100 Scale bar: 50 µm. *Socs36E*, *Suppressor of cytokine signaling at 36E*. **(D)** Box plot shows the
1101 quantitation of the relative fluorescence intensity of 10 kD dextran uptake based on images in
1102 (C); middle line depicts the median and whiskers show Tukey. Statistical analysis was
1103 performed with a two-tailed Student's t-test; ****, P<0.0001; n= 30 from six 1-day-old females
1104 (5 nephrocytes/fly). **(E)** Representative confocal images of 10 kD dextran fluorescence (red)
1105 in nephrocytes from control flies (*ppl*-Gal4/+) and flies with fat body-specific overexpression
1106 of JAK-STAT ligand Upd2 (*ppl*-Gal4>*upd2:GFP*); DAPI (blue) stains DNA to visualize the
1107 nucleus. Scale bar: 50 µm. *ppl*, *pumpless*; *upd2*, *unpaired 2*. **(F)** Box plot shows the
1108 quantitation of the relative fluorescence intensity of 10 kD dextran uptake based on images in
1109 (E); middle line depicts the median and whiskers show Tukey. Statistical analysis was
1110 performed with a two-tailed Student's t-test; ****, P<0.0001; n= 30 from six 1-day-old females
1111 (5 nephrocytes/fly).
1112
1113
1114
1115
1116
1117
1118
1119
1120
1121
1122
1123
1124

Figure 6

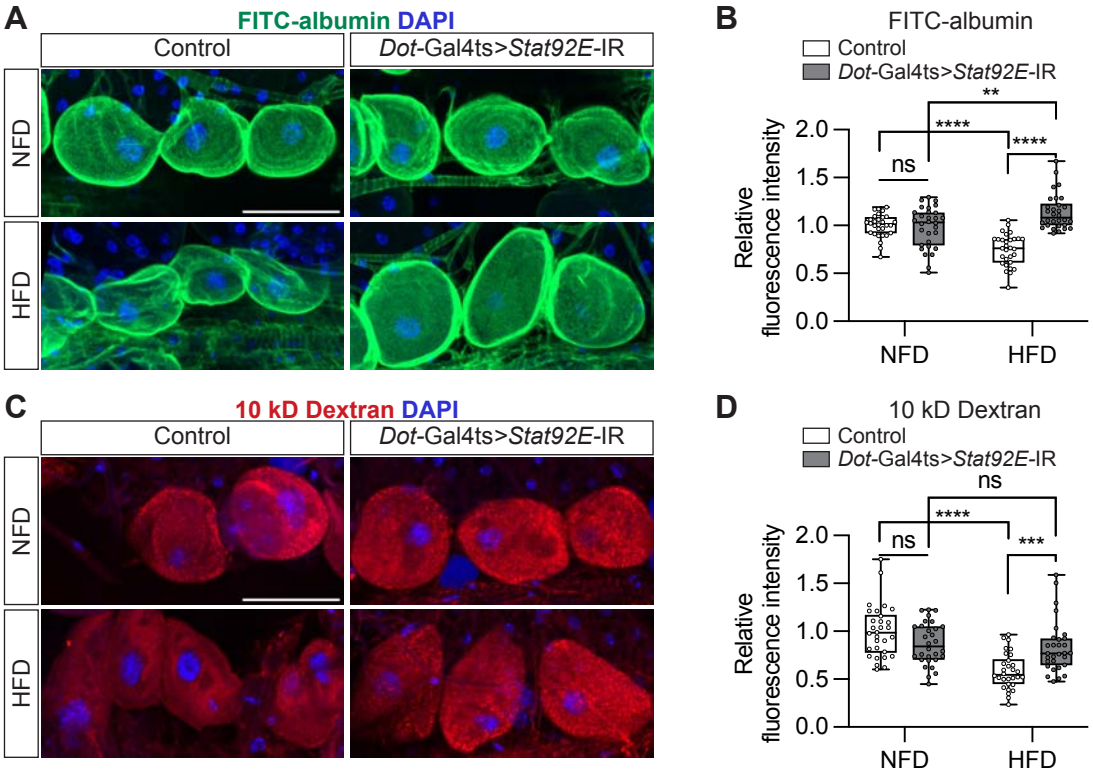
A
FITC-albumin DAPI
Control
Dot-Gal4ts>Stat92E-IR
NFD
HFD
B
FITC-albumin
Control
Dot-Gal4ts>Stat92E-IR
Relative fluorescence intensity
2.0
1.5
1.0
0.5
0.0
ns
****
**
****
NFD
HFD
C
10 kD Dextran DAPI
Control
Dot-Gal4ts>Stat92E-IR
NFD
HFD
D
10 kD Dextran
Control
Dot-Gal4ts>Stat92E-IR
Relative fluorescence intensity
2.0
1.5
1.0
0.5
0.0
ns
ns
****
***
NFD
HFD

1161 **Figure 6. Silencing *Stat92E* attenuates nephrocyte functional defects caused by a high-**
1162 **fat diet**
1163 Nephrocytes from control flies (*Dot*-Gal4/+; *tub*-Gal80ts/+) and those with *Stat92E* silencing
1164 as adults (*Dot*-Gal4/UAS-*Stat92E*-IR; *tub*-Gal80ts/+). UAS-*Stat92E*-RNAi expression was
1165 induced at the adult stage (see Figure 4A) for seven days before the uptake assay. *Stat92E*,
1166 *Singal-transducer and activator of transcription 92E*. **(A)** Representative confocal images of
1167 FITC-albumin fluorescence (green); DAPI (blue) stains DNA to visualize the nucleus. Scale
1168 bar: 50 μm. **(B)** Box plot shows the quantitation of the relative fluorescence intensity of FITC-
1169 albumin uptake based on images in (A); middle line depicts the median and whiskers show
1170 Tukey. Statistical analysis was performed by two-way ANOVA with Sidak correction; **,
1171 P<0.01; ****, P<0.0001; ns, not significant; n = 30 from six 1-day-old females (5
1172 nephrocytes/fly). **(C)** Representative confocal images of 10 kD dextran fluorescence (red);
1173 DAPI (blue) stains DNA to visualize the nucleus. Scale bar: 50 μm. **(D)** Box plot shows the
1174 quantitation of the relative fluorescence intensity of 10 kD dextran uptake based on images in
1175 (C); middle line depicts the median and whiskers show Tukey. Statistical analysis was
1176 performed by two-way ANOVA with Sidak correction; ***, P<0.001; ****, P<0.0001; ns, not
1177 significant; n = 30 from six 1-day-old females (5 nephrocytes/fly).
1178
1179
1180
1181
1182
1183
1184
1185
1186
1187
1188
1189
1190
1191
1192
1193
1194
1195
1196
1197

Figure 7

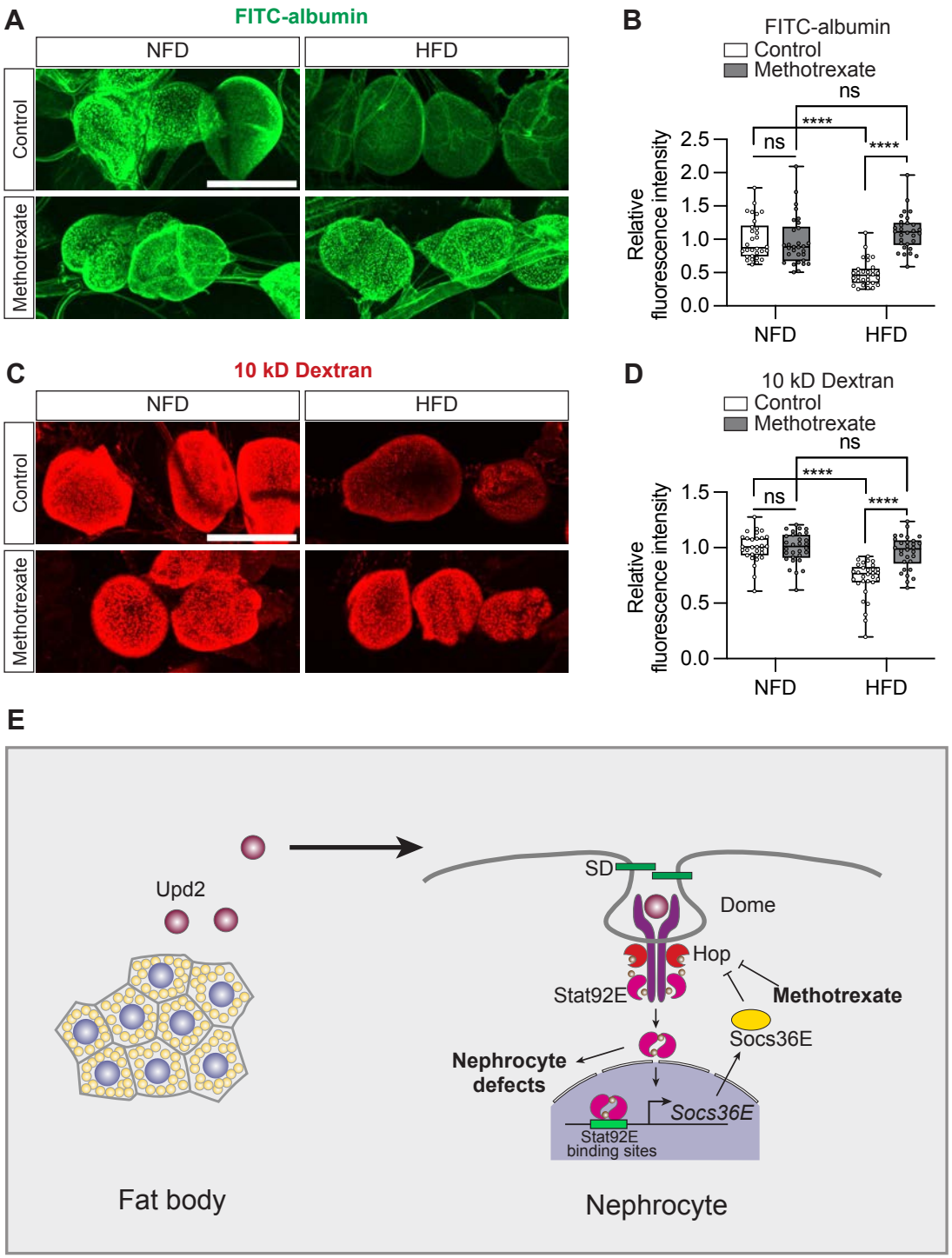
A
FITC-albumin
NFD
HFD
Control
Methotrexate
B
FITC-albumin
Control
Methotrexate
ns
****
ns
****
Relative fluorescence intensity
2.5
2.0
1.5
1.0
0.5
0.0
NFD
HFD
C
10 kD Dextran
NFD
HFD
Control
Methotrexate
D
10 kD Dextran
Control
Methotrexate
ns
****
ns
****
Relative fluorescence intensity
1.5
1.0
0.5
0.0
NFD
HFD
E
Upd2
SD
Dome
Hop
Stat92E
Methotrexate
Socs36E
Nephrocyte defects
Socs36E
Stat92E binding sites
Fat body
Nephrocyte

1235 **Figure 7. Methotrexate treatment can restore nephrocyte function following a high-fat**
1236 **diet**
1237 Nephrocytes from control *Drosophila* (w^{1118}; 7-day-old females) fed a regular diet (normal fat
1238 diet, NFD) or high-fat diet (NFD supplemented with 14% coconut oil, HFD), with or without
1239 methotrexate (10 μM; ex vivo 60 min) treatment. **(A)** Representative confocal images of FITC-
1240 albumin fluorescence (green). Scale bar: 50 μm. **(B)** Box plot shows the quantitation of the
1241 relative fluorescence intensity of FITC-albumin uptake based on images in (A); middle line
1242 depicts the median and whiskers show Tukey. Statistical analysis was performed by two-way
1243 ANOVA with Sidak correction; ****, P<0.0001; ns, not significant; n = 30 from six 1-day-old
1244 females (5 nephrocytes/fly). **(C)** Representative confocal images of 10 kD dextran
1245 fluorescence (red). Scale bar: 50 μm. **(D)** Box plot shows the quantitation of the relative
1246 fluorescence intensity of 10 kD dextran uptake based on images in (C); middle line depicts the
1247 median and whiskers show Tukey. Statistical analysis was performed by Mann-Whitney U
1248 test; ****, P<0.0001; ns, not significant; n = 30 from six 1-day-old females (5 nephrocytes/fly).
1249 **(E)** Graphic of proposed model for high-fat diet-induced nephrocyte defects via an adipose-
1250 nephrocyte axis. A high-fat diet upregulates the expression and secretion of the adipokine
1251 Unpaired 2 (Upd2), leptin-like hormone, from the fat body. Upd2 is a JAK-STAT ligand, and it
1252 activates JAK-STAT signaling at the nephrocytes (Signal-transducer and activator of
1253 transcription 92E, Stat92E; Suppressor of cytokine signaling at 36E, Socs36E; JAK
1254 Hopscotch, Hop; Domeless, Dome). The overactive JAK-STAT pathway disrupts the integrity
1255 of the slit diaphragm (SD) filtration structure and thereby leads to nephrocyte dysfunction.
1256
1257
1258
1259
1260
1261
1262
1263
1264
1265
1266
1267
1268
1269
1270
1271

Supplementary figure S1

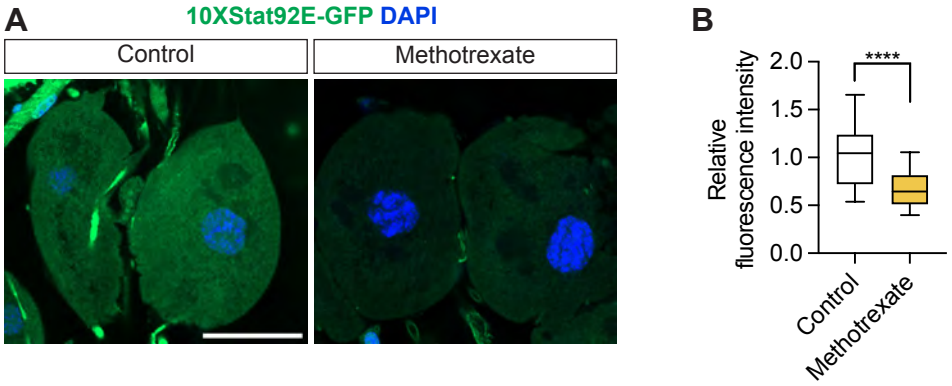

1309 **Supplementary figure S1. Methotrexate treatment inhibits JAK-STAT pathway activity**
1310 **(A)** Representative confocal images of 1-day-old female adult nephrocytes (*10xStat92E*-
1311 GFP). Control, incubated in Schneider's Drosophila Medium (ex vivo for 60 min at room
1312 temperature); methotraxate, incubated in 10 μM methotrexate in Schneider's Drosophila
1313 Medium (ex vivo for 60 min at room temperature). *10xStat92E*-GFP in green fluorescence.
1314 DAPI staining in blue to visualize the nucleus. Scale bar: 20 μm. **(B)** Box plot shows the
1315 quantitation of the relative fluorescence intensity of *10xStat92E*-GFP based on the images in
1316 (A); middle line depicts the median and whiskers show Tukey. Statistical analysis was
1317 performed with a two-tailed t-test; ****, $P<0.0001$; $n = 30$ nephrocytes from six 1-day old female
1318 adults (5 nephrocytes/fly).
1319
1320